EXTENDED PDF FORMAT
SPONSORED BY
SIGMA
Life Science
sigma.com/knockout

Science
AAAS

A Molecular MoS_2 Edge Site Mimic for Catalytic Hydrogen Generation

Hemamala I. Karunadasa, *et al.*

Science **335**, 698 (2012);
DOI: 10.1126/science.1215868

This copy is for your personal, non-commercial use only.

If you wish to distribute this article to others, you can order high-quality copies for your colleagues, clients, or customers by clicking here.

Permission to republish or repurpose articles or portions of articles can be obtained by following the guidelines here.

The following resources related to this article are available online at www.sciencemag.org (this infomation is current as of February 29, 2012):

Updated information and services, including high-resolution figures, can be found in the online version of this article at:
http://www.sciencemag.org/content/335/6069/698.full.html

Supporting Online Material can be found at:
http://www.sciencemag.org/content/suppl/2012/02/09/335.6069.698.DC1.html

This article **cites 35 articles**, 1 of which can be accessed free:
http://www.sciencemag.org/content/335/6069/698.full.html#ref-list-1

This article appears in the following **subject collections:**
Chemistry
http://www.sciencemag.org/cgi/collection/chemistry

Downloaded from www.sciencemag.org on February 29, 2012

Science (print ISSN 0036-8075; online ISSN 1095-9203) is published weekly, except the last week in December, by the American Association for the Advancement of Science, 1200 New York Avenue NW, Washington, DC 20005. Copyright 2012 by the American Association for the Advancement of Science; all rights reserved. The title *Science* is a registered trademark of AAAS.

difference spectra are quite simple, with only one main band (or very close doublet) affected by substitution. Consequently, only one dominant configuration (with minor conformers arising from remote group orientation) is adopted upon extraction from solution. It is possible that removal of solvent changes the structure, and that the active species in solution could be electrically neutral, and both of these issues can be addressed with the cryogenic approach by retaining many solvent molecules and working with bulky noncoordinating counterions such as tetramethyl ammonium to explore the neutral adduct. It is nonetheless an important first step to establish that in the protonated adduct characterized here, the substrate (**S**) adopts a configuration consistent with the observed enantioselectivity of the catalyst (*2*, *5*).

The pivotal assignment of the strong contact occurring between N-H$^+$ and CO_2H in **C-S** relies solely on the behavior of the ^{13}C label in the acid position. This raises the importance of not only identifying whether particular groups are involved in H-bonding, but also establishing specifically which donors and acceptors are paired, at least in one contact point. One avenue to explore, therefore, is whether the intensities of both the donor and acceptor bonds can be modulated by the isotopic labeling scheme. An attractive possibility in this regard would be to monitor the combination band involving one quantum in both the donor and acceptor groups (e.g., N-H and C=O), which one would expect to be activated by the anharmonic coupling inherent in the H-bond. The presence of an isotope shift from both ^{15}N and ^{13}C labels would then confirm a specific point contact.

This procedure yields a microscopic picture of a docking arrangement, sufficiently constraining the possible structures such that electronic structure theory can be efficiently used to converge on a unique minimum-energy structure within an otherwise computationally prohibitive, high-dimensionality landscape. The method appears general and likely to become a central tool for the characterization of processes that depend on supramolecular associations.

References and Notes

1. D. H. Williams, B. Bardsley, *Angew. Chem. Int. Ed.* **38**, 1173 (1999).
2. J. L. Gustafson, D. Lim, S. J. Miller, *Science* **328**, 1251 (2010).
3. M. S. Taylor, E. N. Jacobsen, *Angew. Chem. Int. Ed.* **45**, 1520 (2006).
4. A. G. Doyle, E. N. Jacobsen, *Chem. Rev.* **107**, 5713 (2007).
5. J. L. Gustafson, D. Lim, K. T. Barrett, S. J. Miller, *Angew. Chem. Int. Ed.* **50**, 5125 (2011).
6. J. M. Lehn, *Proc. Natl. Acad. Sci. U.S.A.* **99**, 4763 (2002).
7. K. H. Bleicher, H. J. Böhm, K. Müller, A. I. Alanine, *Nat. Rev. Drug Discov.* **2**, 369 (2003).
8. J. Bajorath, *Nat. Rev. Drug Discov.* **1**, 882 (2002).
9. W. L. Jorgensen, *Science* **303**, 1813 (2004).
10. B. K. Shoichet, *Nature* **432**, 862 (2004).
11. L. J. Prins, D. N. Reinhoudt, P. Timmerman, *Angew. Chem. Int. Ed.* **40**, 2382 (2001).
12. S. Ham, S. Cha, J. H. Choi, M. Cho, *J. Chem. Phys.* **119**, 1451 (2003).
13. C. L. Perrin, J. B. Nielson, *Annu. Rev. Phys. Chem.* **48**, 511 (1997).
14. G. A. Jeffrey, W. Saenger, *Hydrogen Bonding in Biological Structures* (Springer-Verlag, Berlin, New York, 1991).
15. P. I. Haris, G. T. Robillard, A. A. van Dijk, D. Chapman, *Biochemistry* **31**, 6279 (1992).
16. S. Sonar *et al.*, *Nat. Struct. Biol.* **1**, 512 (1994).
17. L. Tadesse, R. Nazarbaghi, L. Walters, *J. Am. Chem. Soc.* **113**, 7036 (1991).
18. R. R. Knowles, E. N. Jacobsen, *Proc. Natl. Acad. Sci. U.S.A.* **107**, 20678 (2010).
19. M. Z. Kamrath, R. A. Relph, T. L. Guasco, C. M. Leavitt, M. A. Johnson, *Int. J. Mass Spectrom.* **300**, 91 (2011).
20. M. Z. Kamrath *et al.*, *J. Am. Chem. Soc.* **133**, 6440 (2011).
21. M. Okumura, L. I. Yeh, J. D. Myers, Y. T. Lee, *J. Chem. Phys.* **85**, 2328 (1986).
22. D. J. Goebbert, T. Wende, R. Bergmann, G. Meijer, K. R. Asmis, *J. Phys. Chem. A* **113**, 5874 (2009).
23. T. R. Rizzo, J. A. Stearns, O. V. Boyarkin, *Int. Rev. Phys. Chem.* **28**, 481 (2009).
24. J. A. Stearns *et al.*, *J. Am. Chem. Soc.* **129**, 11814 (2007).
25. L. Wang *et al.*, *J. Am. Chem. Soc.* **133**, 16062 (2011).
26. J. A. Stearns, C. Seaiby, O. V. Boyarkin, T. R. Rizzo, *Phys. Chem. Chem. Phys.* **11**, 125 (2009).
27. R. R. Gardner, G. B. Liang, S. H. Gellman, *J. Am. Chem. Soc.* **117**, 3280 (1995).
28. C. P. Rao, R. Nagaraj, C. N. R. Rao, P. Balaram, *Biochemistry* **19**, 425 (1980).
29. D. Semrouni *et al.*, *J. Am. Soc. Mass Spectrom.* **21**, 728 (2010).
30. R. C. Dunbar, J. D. Steill, J. Oomens, *Int. J. Mass Spectrom.* **297**, 107 (2010).
31. B. M. Elliott *et al.*, *J. Chem. Phys.* **129**, 094303 (2008).
32. J. M. Bakker, L. Mac Aleese, G. von Helden, G. Meijer, *J. Chem. Phys.* **119**, 11180 (2003).
33. S. G. Stepanian, I. D. Reva, E. D. Radchenko, G. G. Sheina, *Vib. Spectrosc.* **11**, 123 (1996).
34. Y. Inokuchi, N. Nishi, *J. Phys. Chem. A* **107**, 11319 (2003).
35. H. M. Lee *et al.*, *Phys. Chem. Chem. Phys.* **12**, 6278 (2010).
36. E. P. L. Hunter, S. G. Lias, *J. Phys. Chem. Ref. Data* **27**, 413 (1998).

Acknowledgments: M.A.J. thanks the Air Force Office of Scientific Research under grant FA-9550-09-1-0139. We also thank the U.S. NSF under grants CHE-091199 (M.A.J.) and CHE-0848242 (A.B.M.). S.J.M thanks the NIH under grant R01-GM068649. This work was supported in part by the Yale University Faculty of Arts and Sciences High Performance Computing facility (and staff).

Supporting Online Material
www.sciencemag.org/cgi/content/full/science.1214948/DC1
Materials and Methods
Figs. S1 to S9
References (*37–40*)

7 October 2011; accepted 20 December 2011
Published online 19 January 2012;
10.1126/science.1214948

A Molecular MoS_2 Edge Site Mimic for Catalytic Hydrogen Generation

Hemamala I. Karunadasa,[1,2] Elizabeth Montalvo,[1] Yujie Sun,[1,2] Marcin Majda,[1] Jeffrey R. Long,[1,3]* Christopher J. Chang[1,2,4]*

Inorganic solids are an important class of catalysts that often derive their activity from sparse active sites that are structurally distinct from the inactive bulk. Rationally optimizing activity is therefore beholden to the challenges in studying these active sites in molecular detail. Here, we report a molecule that mimics the structure of the proposed triangular active edge site fragments of molybdenum disulfide (MoS_2), a widely used industrial catalyst that has shown promise as a low-cost alternative to platinum for electrocatalytic hydrogen production. By leveraging the robust coordination environment of a pentapyridyl ligand, we synthesized and structurally characterized a well-defined Mo^{IV}-disulfide complex that, upon electrochemical reduction, can catalytically generate hydrogen from acidic organic media as well as from acidic water.

Molybdenite, or molybdenum disulfide (MoS_2), the earliest form of molybdenum to be identified from ores, is one of the most widely used catalysts in industry today as the standard for hydrodesulfurization (HDS) of petroleum (*1*). In its nanoparticulate form, MoS_2 has further demonstrated promise as an inexpensive alternative to platinum for the electrochemical and photochemical generation of hydrogen from water (*2*–*6*). As is the case with many inorganic solids, the catalytic activity of MoS_2 is localized to rare surface sites, whereas the bulk material is relatively inert (*7*–*9*). High-resolution scanning tunneling microscopy studies and theoretical calculations performed on nanoparticulate MoS_2 structures that form under sulfiding conditions implicate the formation of disulfide linkages or triangular MoS_2 units along the fully sulfided catalytically active edges of the layered structure (*10*–*14*). However, the precise molecular structures and modes of action of these sites remain elusive. Because of the bulk material's layered structure, which favors the growth of plate-like crystals, a single crystal with a large edge dimension is extremely challenging to prepare (*1*). Here, we report the synthesis of a well-defined molecular analog of the proposed MoS_2 edge structure, a side-on bound Mo^{IV}-disulfide complex. Electrochemical reduction of this mol-

---

[1] Department of Chemistry, University of California, Berkeley, CA 94720, USA. [2] Chemical Sciences Division, Lawrence Berkeley National Laboratory, Berkeley, CA 94720, USA. [3] Materials Sciences Division, Lawrence Berkeley National Laboratory, Berkeley, CA 94720, USA. [4] Howard Hughes Medical Institute, University of California, Berkeley, CA 94720, USA.

*To whom correspondence should be addressed. E-mail: chrischang@berkeley.edu (C.J.C.); jrlong@berkeley.edu (J.R.L.)

ecule leads to the catalytic generation of hydrogen from acidic organic media as well as from acidic water, lending support to the proposed active site morphology in the more active heterogeneous catalyst.

Recent efforts from our laboratories have explored the chemistry of the $PY5Me_2$ ligand [$PY5Me_2$ = 2,6-bis(1,1-bis(2-pyridyl)ethyl)pyridine] and the ability of its Mo^{IV}-oxo complex $[(PY5Me_2)MoO]^{2+}$ to catalyze the production of hydrogen from neutral water (*15*). Along these lines, treatment of the Mo^{II} precursor $[(PY5Me_2)Mo(CF_3SO_3)]^{1+}$ with S_8 at room temperature affords the Mo^{IV}-disulfide complex $[(PY5Me_2)MoS_2]^{2+}$ (**1**) in 74% yield (Fig. 1) (*16*). This molecule represents a rare species in molybdenum coordination chemistry (*17*–*20*) and a discrete molecular analog of the proposed triangular MoS_2 edge sites of molybdenite. A single-crystal x-ray analysis of **1** revealed a distorted pseudo-octahedral geometry around the metal center, with the MoS_2 plane twisting away from the plane of the axial pyridyl ligand by approximately 46°. The $PY5Me_2$ ligand is slightly distorted around the central metal with a mean Mo-N distance of 2.19(2) Å and a mean N-Mo-N angle of 82(6)°. The mean Mo-S distance of 2.402(2) Å, S-S distance of 2.019(1) Å and S-Mo-S angle of 49.68(3)° are similar to those reported for $Cp^*{}_2MoS_2$ (*21*) and $Cp^{tBu}{}_2MoS_2$ (*22*), and together frame a molecular MoS_2 isosceles triangle supported by the $PY5Me_2$ ligand. The longer Mo-S distance compared with the 2.254(2) Å bond length for a terminal sulfido ligand bonded to Mo^{IV} (*18*) indicates single Mo-S bonds. Similarly, the S-S bond length is close to the distance of 2.060 Å observed between S atoms in S_8 (*23*) as well as the distance between S atoms in a dinuclear Mo^V complex bearing a μ-$S_2{}^{2-}$ bridging ligand (*24*), consistent with a single bond between the two S atoms.

The cyclic voltammogram on a glassy carbon disc electrode (GCDE) of a 1-mM solution of **1** in acetonitrile with 0.1 M of $(Bu_4N)PF_6$ electrolyte shows a reversible set of redox peaks at $E_{1/2}$ = 1.27 V versus the standard hydrogen electrode (SHE) (Fig. 2A), which we assigned to the $[(PY5Me_2)MoS_2]^{2+/3+}$ couple. Scanning cathodically reveals two more reversible redox couples at $E_{1/2}$ = –0.20 and –0.82 V versus SHE assigned to the $[(PY5Me_2)MoS_2]^{2+/1+}$ and $[(PY5Me_2)MoS_2]^{1+/0}$ couples. At still more negative potentials, a larger irreversible wave rising to a maximum at E_p = –1.49 V versus SHE is presumably due to an electrochemical-chemical (EC) process, perhaps involving the $S_2{}^{2-}$ ligand (fig. S2).

The accessibility of multiply reduced states for the $Mo^{IV}S_2$ complex **1** prompted us to investigate its ability to reduce protons in organic solvents. The cyclic voltammogram (on a GCDE) of a 0.5-mM solution of **1** in acetonitrile containing 79 mM (160 equivalents) of acetic acid shows a sharp catalytic current after the $Mo^{III/II}$ couple with an onset potential of about –1.00 V versus SHE. The current reaches half its maximum value at –1.27 V and peaks at –1.50 V versus SHE. (Fig. 2B). The peak currents of the precatalytic waves as well as the catalytic wave vary linearly with the square root of the scan rate (fig. S4), indicating diffusion-limited redox processes, with the electrochemically active species freely diffusing in solution. The catalytic nature of the reductive wave at about –1.27 V versus SHE was verified by passing 3.00 C of charge during a bulk electrolysis. The experiment was conducted on a 55-μM solution of **1** in acetonitrile with 9 mM of acetic acid, using a glassy carbon plate electrode in a double compartment cell with the potential held at –1.09 V versus SHE for 2.75 hours. A control experiment performed under identical conditions, but without **1**, showed the accumulation of just 0.679 C of charge (fig. S5). Subtracting the background contribution of direct acid reduction leads to 10.9 equiv. of charge generated per molybdenum center, which precludes a stoichiometric reaction with respect to molybdenum. Gas chromatography of the headspace gas during the bulk electrolysis confirmed the generation of H_2.

Encouraged by this clear indication that **1** can operate as a molecular electrocatalyst in acetonitrile, we chose to explore its potential utility for the electrocatalytic reduction of protons in water, a much more attractive medium for the sustainable generation of hydrogen. Indeed, a sharp increase in current, indicative of catalytic water reduction, is evident in cyclic voltammograms (on a GCDE) of aqueous solutions of **1** at pH values of 3, 4, 5, and 6, with optimal activity observed at pH 3. We therefore conducted subsequent studies in aqueous media at pH 3 using potassium hydrogen phthalate (KHP) or sodium acetate aqueous buffers. The voltammogram (on a GCDE) of a 1.2-mM solution of **1** in aqueous acetate buffer at pH 3, acquired at a scan rate of 0.1 V/s, shows two irreversible reductions at peak potentials of −0.34 and −0.53 V versus SHE, respectively, before the onset of the catalytic current at a potential of about −0.65 V versus SHE (Fig. 2C). The voltammogram of the molybdenum-oxo compound $[(PY5Me_2)MoO]^{2+}$, taken under identical conditions, shows no catalytic activity within the solvent electrochemical window, confirming that the sulfide ligands are not hydrolyzed under acidic aqueous conditions. As observed in acetonitrile solution, the current response of the redox events of **1** on the glassy carbon electrode in acidic water shows a linear dependence on the square root of the scan rate, which is indicative of a diffusion-controlled process (figs. S6 and S7). A controlled potential electrolysis of a 92-μM solution of **1** in 3 M aqueous acetate buffer at pH 3 conducted using a glassy carbon rod electrode in a double-compartment cell at −0.75 V versus SHE for 1 hour led to the accumulation of 2.42 C of charge. In the absence of **1**, an identical experiment led to the passage of only 0.015 C of charge (fig. S8). Subtraction of this background activity affords 14.3 equiv. of charge per molybdenum center, establishing the catalytic nature of the reduction. To determine whether deposition on the electrode occurs during an extended electrolysis, the electrode was carefully rinsed with distilled water and examined using molybdenum K-edge x-ray absorption spectroscopy, which indicated no molybdenum species present to the limit of x-ray fluorescence measurement (monolayer). Furthermore, the electronic adsorption spectra of the solution before and after the 1-hour electrolysis show that the $(PY5Me_2)Mo$ unit remains intact during that period (fig. S9).

Because of the background activity of direct water reduction at the glassy carbon electrode at high overpotentials, subsequent experiments were conducted on a mercury electrode, where no direct water reduction occurs below overpotentials of about −1 V (overpotential being the difference between the applied potential and the thermodynamic potential for water reduction at the same pH) (*25*). Similar to the data obtained on a glassy carbon electrode, a cyclic voltammogram on a mercury drop electrode recorded at a

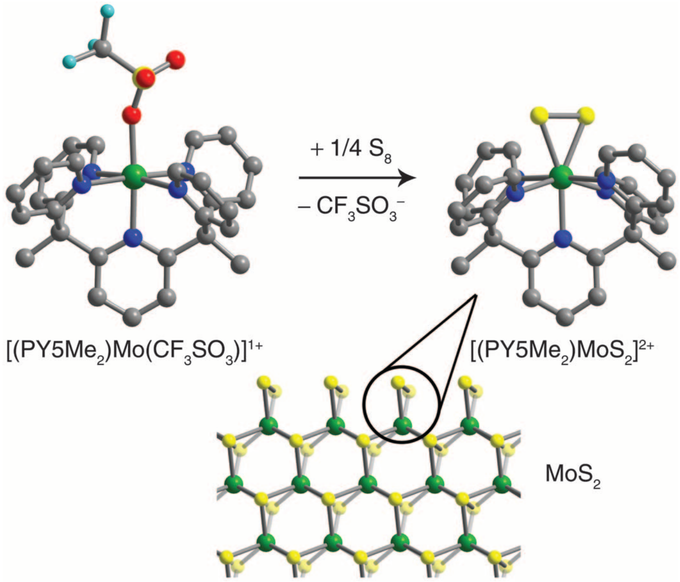

Fig. 1. Reaction of $[(PY5Me_2)Mo(CF_3SO_3)]^{1+}$ with sulfur to form $[(PY5Me_2)MoS_2]^{2+}$ (**1**, top), and a model of the layered structure of MoS_2 (bottom), highlighting the proposed surface reconstruction to give disulfide-terminated edge sites. The molecular structures depicted at the top are the results of single-crystal x-ray analyses. Green, yellow, light blue, red, blue, and gray spheres represent Mo, S, F, O, N, and C atoms, respectively; H atoms are omitted for clarity.

scan rate of 0.5 V/s shows two reductions, with a sharp wave corresponding to the first reduction at –0.16 V versus SHE, followed by a quasireversible couple at $E_{1/2}$ = –0.38 V preceding the catalytic current (Fig. 2D). To probe the nature of the first reduction process, we investigated the pH dependence of the cathodic peak potential (V_c), summarized in the Pourbaix diagram depicted in Fig. 4 (assuming electrochemical reversibility for this redox couple). Here, V_c declines linearly with rising solution pH at a slope of –59.8 (±0.8), which is within experimental error of the ideal value of –59 mV, corresponding to the association of one proton with the electron transfer (*25*). The observed pH dependence, taken together with the irreversibility of this peak, suggests a geometric distortion about the metal center consistent with the formation of a protonated reduced Mo-disulfide unit or cleavage of a Mo-S bond. Formation of a S-H bond is the first step in the proposed pathway for electrocatalytic proton reduction at MoS_2 nanoparticle edge sites (*10*), as well as in dinuclear $(CpMo\mu\text{-}S)_2S_2CH_2$ complexes (*26*). Protonation of the bridging sulfido ligand is also proposed for H_2 evolution by the nitrogenase enzyme (*27*). Furthermore, terminal S-H bonds at the edges of MoS_2 HDS catalysts have been assigned, which has led to speculation that such species are the source of H_2 for the hydrogenation of the desulfurized molecules (*28*). In contrast, the second reductive wave does not show a similar pH dependence, leading us to hypothesize that this process involves one electron reduction of the complex, which upon subsequent reduction and protonation forms the catalytically active species. Close contact between metal centers adsorbed on the electrode may also facilitate a multinuclear pathway, perhaps through the formation of S-H bonds that could homolytically or heterolytically cleave to yield H_2.

Analysis of the peak current of the cathodic and anodic scans of the second quasireversible redox couple as a function of scan rate (fig. S10) shows a linear relation, consistent with adsorption of the molecules on the electrode surface. Stabilization of the reduced molybdenum complexes through adsorption on the Hg electrode would be consistent with the positive shift of the redox events compared with the diffusion-limited redox processes observed with glassy carbon electrodes (*25*). For an idealized adsorption, which assumes reversible electron transfer with no interaction between adsorbed species, the number of electrons that give rise to the wave corresponds to 90.6/$\Delta E_{p,1/2}$, where $\Delta E_{p,1/2}$ is the width of the wave at half the maximum current (*25*). At scan rates of 200 to 1000 mV/s, a mean width of 74(2) mV is observed for the anodic scan, which indicates a one-electron process. By observing the current response to variations in scan rate, we can quantify the coverage of metal sites on the electrode surface to be 3.4 to 3.6 × 10^{-10} mols/cm^2. A rough calculation of the footprint of **1**, obtained using the dimensions from the crystal structure, suggests monolayer coverage on the electrode [see supporting online material (SOM)]. Due to possible increases in surface area of the mercury when the pool is stirred during electrolysis, we use an estimated surface coverage of 10^{-10} mols/cm^2 for subsequent hydrogen evolution rate calculations.

The cyclic voltammogram of a 130-μM solution of **1** at pH 3 shows a catalytic current with an overpotential of about −400 mV (−0.58 V versus SHE) (Fig. 3B). The catalytic performance of $[(PY5Me_2)MoO]^{2+}$ was once again evaluated at the same pH to establish that **1** did not form the molybdenum-oxo complex under aqueous, reducing conditions. As depicted in Fig. 3B, $[(PY5Me_2)MoO]^{2+}$ shows the onset of a catalytic current at an overpotential of −700 mV (−0.88 V versus SHE) under the same conditions. Thus, using the disulfide complex **1** gives an improvement of 300 mV in overpotential with respect to the analogous oxo complex for water reduction at pH 3. Controlled potential electrolysis experiments were conducted to assess the rate of hydrogen production at various overpotentials. Identical measurements were performed with and without the catalyst to subtract the background activity at each applied potential. Figure S11 shows the charge accumulated over 1-min intervals, with applied overpotential increasing from −428 mV until a saturation value of 6.36 C is reached at −828 mV (due to the voltage between the working and auxiliary electrodes exceeding the maximum voltage obtainable by the potentiostat at high current densities). Under these conditions, the pH change of the solution, as well as quantitative gas chromatographic analysis of the electrolysis-cell headspace, indicated that the catalyst performs at close to 100% Faradaic efficiency, where every electron is used for the generation of hydrogen (see figs. S12 and S13 and SOM). At an overpotential of −828 mV, the observed turnover frequency (TOF) reached a maximum of 280 moles of H_2 per mole of catalyst per second.

We also evaluated the catalytic properties of **1** using a sample of California seawater, which was buffered at pH 3 by the addition of acetic acid and sodium acetate. As shown in Fig. 3C, the rates of hydrogen evolution for a given overpotential were similar to those observed in the studies conducted in distilled water, but with an even higher optimal TOF of 480 moles of H_2 per mole of catalyst per second at an overpotential of −780 mV. This result highlights the robustness of the catalyst to the impurities found in seawater.

To assess the long-term stability of the catalyst, an extended electrolysis was conducted in a 3 M pH 3 acetate buffer at an overpotential of

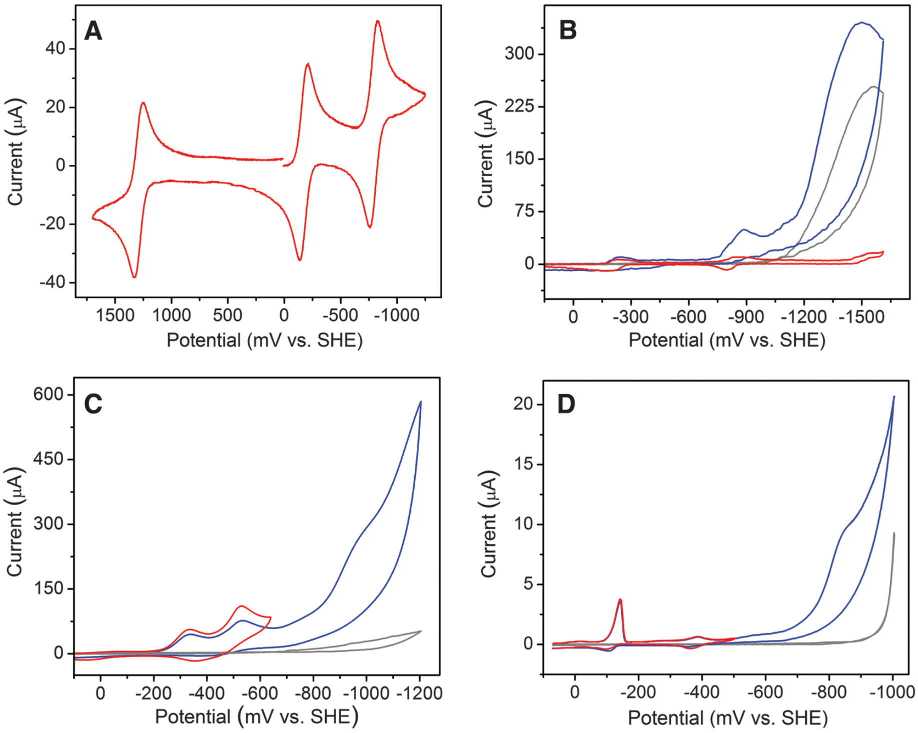

Fig. 2. Cyclic voltammograms on a glassy carbon disc electrode (*A* = 7.07 × 10^{-2} cm^2) of (**A**) an acetonitrile solution containing 1 mM of $[(PY5Me_2)MoS_2](CF_3SO_3)_2$ (**1**) and 0.1 M of $(Bu_4N)PF_6$ at a scan rate of 0.1 V/s; (**B**) acetonitrile solutions containing 0.5 mM of **1** and 0.1 M of $(Bu_4N)PF_6$ in the presence (blue line) and absence (red line) of 160 equiv. of acetic acid (79 mM), or 79 mM of the acid alone (gray line), at a scan rate of 0.1 V/s; (**C**) 1 M aqueous acetate buffer at pH 3 in the presence (red and blue lines) and absence (gray line) of 1.1 mM of **1** at a scan rate of 0.1 V/s. (**D**) Cyclic voltammograms on a mercury drop electrode (*A* ~ 1.16 × 10^{-2} cm^2) of 0.05 M aqueous KHP buffer at pH 3 in the presence (red and blue lines) and absence (gray line) of 160 μM of **1** at a scan rate of 0.5 V/s. In (C) and (D), the red line indicates the initial scan and the blue line indicates the subsequent scan.

−780 mV (Fig. 3D). The total turnover number (TON) reached ~3.5×10^3 moles of H_2 per mole of catalyst, showing that the catalyst is stable for long durations in aqueous media. This value is the lower bound for the catalyst lifetime using the total number of molecules in solution. Calculating the TON using the surface coverage of catalyst molecules on the electrode affords 1.9×10^7 moles of H_2 per mole of catalyst. We report both numbers because we do not yet know the rate of exchange of the surface layer with the molecules in solution during the 23-hour period.

Comparing the electronic adsorption spectrum of a solution of the catalyst electrolyzed for 1 hour against a control shows that the $(PY5Me_2)Mo$ unit remains intact during this period (fig. S14).

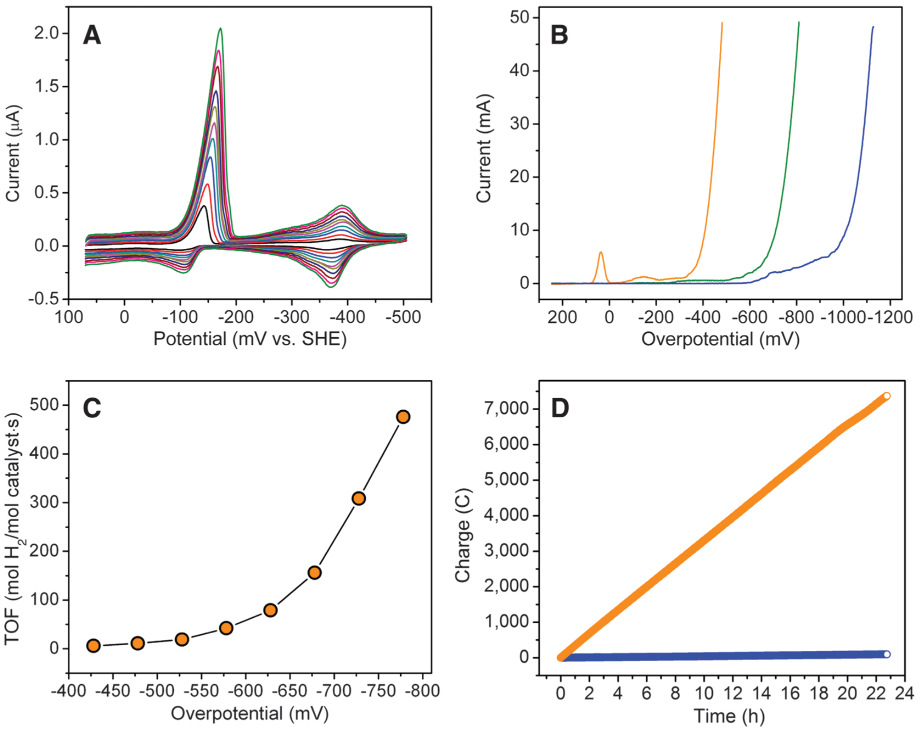

Fig. 3. (**A**) Scan rate dependence of precatalytic waves for a 160-µM solution of $[(PY5Me_2)MoS_2](CF_3SO_3)_2$ (**1**) in 0.05 M aqueous KHP buffer at pH 3, at scan rates ranging from 100 to 1000 mV/s in 100 mV/s increments on a mercury drop electrode (A ~ 11.6×10^{-3} cm^2). (**B**) Cathodic scans of 130-µM solutions of **1** (orange line) or $[(PY5Me_2)MoO](CF_3SO_3)_2$ (green line) in 1 M aqueous acetate buffer at pH 3 and of the buffer solution alone (blue line), on a mercury pool electrode (A = 19.6 cm^2) at a scan rate of 100 mV/s. (**C**) TOF versus overpotential for a 170-µM solution of **1** in seawater maintained at pH 3 with 1 M acetate buffer. The background solvent activity has been subtracted from the data. (**D**) Charge buildup over time from electrolysis of a 66-µM solution of **1** (orange circles) in 3 M aqueous acetate buffer at pH 3, compared with the electrolyte solution alone (blue circles), with the cell operating at an overpotential of −780 mV. Overpotential = applied potential − E(pH 3).

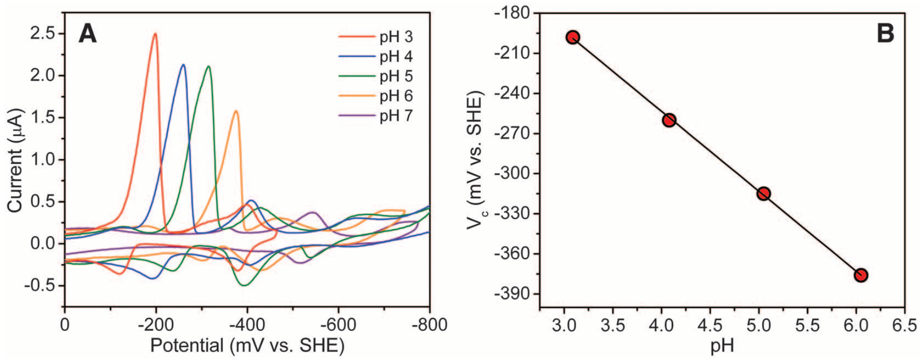

Fig. 4. (**A**) Cyclic voltammograms of 0.3-mM solutions of $[(PY5Me_2)MoS_2](CF_3SO_3)_2$ (**1**) in 0.05 M aqueous KHP buffers at pH values ranging from 3 to 7 on a Hg drop electrode at a scan rate of 1 V/s. (**B**) Pourbaix diagram showing the dependence of the peak potential of the first reductive wave on the solution pH: A linear fit gives a slope of −59.8 (± 0.8).

In addition, a ^1H nuclear magnetic resonance study to quantify the amount of free ligand in solution after a 12-hour electrolysis indicated that less than 3% is lost from the initial catalyst loading, further supporting the stability of this molecular species under reductive, aqueous conditions (see SOM for details). However, adsorption on the mercury surface complicates the characterization of the catalytically active species, which we cannot as yet unambiguously identify. The analogous studies performed using glassy carbon electrodes in organic and aqueous media, where the catalyst is not adsorbed on the electrode surface, support a molecular species as a competent catalyst.

This first-generation molybdenum-disulfide complex exhibits considerably higher stability and comparable TOFs to hydrogenase enzymes (which show rates from 10^2 to 10^4 s^{-1}) (*29*, *30*), albeit with greater overpotentials. For comparison, water-tolerant cobalt-based molecular catalysts attached to glassy carbon electrodes can achieve TOFs of ~90 s^{-1} at an overpotential of −400 mV (*31*), and experimentally determined TOFs ranging from 2.3×10^{-4} to 2.2×10^{-3} s^{-1} at overpotentials ranging from −690 to −1040 mV have been reported for a cobalt complex on a mercury electrode (*32*); an analogous Co complex bearing the $PY5Me_2$ ligand shows a TOF of ~0.3 s^{-1} at an overpotential of −900 mV on a mercury electrode (*33*). Furthermore, TOFs of ~0.07 s^{-1} at the equilibrium potential have been reported for carbon-supported $[Mo_3S_4]^{4+}$ clusters (*34*), which are susceptible to desorption from the electrode. Other examples of molecular catalysts attached to electrodes display lower activity and lifetimes in aqueous solution (*35*–*37*). A key advantage of **1** is the ability to form a layer of MoS_2 units, analogous to constructing a sulfided edge of MoS_2, where the dimensions of the layer can be defined by the size and shape of the electrode. Here, the electronic structure of the MoS_2 units, and thereby perhaps the activity, stability, and required overpotential for proton reduction, may be adjusted through ligand modifications accessible through synthetic chemistry.

The ability to prepare, characterize, and evaluate molecular analogs of the active components of inorganic solids has broad implications for the design and optimization of functional metal sites, not the least of which is control over the density of these units. For example, recent electronic structure calculations conducted on nanoparticulate MoS_2 indicate that only a quarter of the edge sites are used for hydrogen production (*10*). Increasing the number of active edge sites per unit volume by tailoring progressively smaller nanostructures or changing the electronics of the system to increase the enthalpy of hydrogen adsorption is a major challenge in inorganic materials and nanoscience. We present an alternative strategy using discrete molecular units, which in principle can be tailored to give a high density of catalytically active metal sites without the rest of the inactive bulk material.

References and Notes

1. R. Prins, V. H. J. De Beer, G. A. Somorjai, *Catal. Rev. Sci. Eng.* **31**, 1 (1989).
2. B. Hinnemann *et al.*, *J. Am. Chem. Soc.* **127**, 5308 (2005).
3. T. F. Jaramillo *et al.*, *Science* **317**, 100 (2007).
4. Y. Li *et al.*, *J. Am. Chem. Soc.* **133**, 7296 (2011).
5. X. Zong *et al.*, *J. Am. Chem. Soc.* **130**, 7176 (2008).
6. D. Merki, S. Fierro, H. Vrubel, X. Hu, *Chem. Sci.* **2**, 1262 (2011).
7. G. A. Somorjai, M. A. Van Hove, *Prog. Surf. Sci.* **30**, 201 (1989).
8. S. T. Ceyer, *Annu. Rev. Phys. Chem.* **39**, 479 (1988).
9. G. Ertl, *Angew. Chem. Int. Ed. Engl.* **29**, 1219 (1990).
10. B. Hinnemann *et al.*, *J. Am. Chem. Soc.* **127**, 5308 (2005).
11. J. V. Lauritsen *et al.*, *J. Catal.* **221**, 510 (2004).
12. J. C. Duchet, E. M. van Oers, V. H. J. de Beer, R. Prins, *J. Catal.* **80**, 386 (1983).
13. J. V. Lauritsen *et al.*, *Nat. Nano.* **2**, 53 (2007).
14. L. P. Hansen *et al.*, *Angew. Chem. Int. Ed. Engl.* **50**, 10153 (2011).
15. H. I. Karunadasa, C. J. Chang, J. R. Long, *Nature* **464**, 1329 (2010).
16. F. Gloaguen, T. B. Rauchfuss, *Chem. Soc. Rev.* **38**, 100 (2009).
17. S. J. Smith, C. M. Whaley, T. B. Rauchfuss, S. R. Wilson, *Inorg. Chem.* **45**, 679 (2006).
18. V. J. Murphy, G. Parkin, *J. Am. Chem. Soc.* **117**, 3522 (1995).
19. F. A. Cotton, G. Schmid, *Inorg. Chem.* **36**, 2267 (1997).
20. H. Kopf, S. K. S. Hazari, M. Leitner, *Z. Naturforsch. B: Chem. Sci.* **33b**, 1398 (1978).
21. J. H. Shin, D. G. Churchill, B. M. Bridgewater, K. Pang, G. Parkin, *Inorg. Chim. Acta* **359**, 2942 (2006).
22. J. H. Shin *et al.*, *J. Chem. Soc. Dalton Trans.* **11**, 1732 (2001).
23. A. F. Wells, *Structural Inorganic Chemistry* (Clarendon Press, Oxford, ed. 4, 1975).
24. P. D. Smith, D. A. Slizys, G. N. George, C. G. Young, *J. Am. Chem. Soc.* **122**, 2946 (2000).
25. A. J. Bard, L. R. Faulkner, *Electrochemical Methods* (Wiley, New York, 1980).
26. A. M. Appel, D. L. DuBois, M. R. DuBois, *J. Am. Chem. Soc.* **127**, 12717 (2005).
27. I. Dance, *J. Am. Chem. Soc.* **127**, 10925 (2005).
28. N. Y. Topsoe, H. Topsoe, *J. Catal.* **139**, 641 (1993).
29. M. Frey, *ChemBioChem* **3**, 153 (2002).
30. J. A. Cracknell, K. A. Vincent, F. A. Armstrong, *Chem. Rev.* **108**, 2439 (2008).
31. L. A. Berben, J. C. Peters, *Chem. Commun.* **46**, 398 (2010).
32. B. D. Stubbert, J. C. Peters, H. B. Gray, *J. Am. Chem. Soc.* **133**, 18070 (2011).
33. Y. Sun *et al.*, *J. Am. Chem. Soc.* **133**, 9212 (2011).
34. T. F. Jaramillo *et al.*, *J. Phys. Chem. C* **112**, 17492 (2008).
35. R. M. Kellett, T. G. Spiro, *Inorg. Chem.* **24**, 2378 (1985).
36. B. J. Fisher, R. Eisenberg, *J. Am. Chem. Soc.* **102**, 7361 (1980).
37. P. V. Bernhardt, L. A. Jones, *Inorg. Chem.* **38**, 5086 (1999).

Acknowledgments: Initial synthetic and electrochemical studies were supported by the Department of Energy (DOE) Lawrence Berkeley National Laboratory Helios Solar Energy Research Center (51HE112B to C.J.C.). Further electrochemical studies are based on work performed by the Joint Center for Artificial Photosynthesis, a DOE Energy Innovation Hub, supported through the Office of Science of the U.S. Department of Energy under award DE-SC0004993 (J.R.L.). C.J.C. is an investigator with the Howard Hughes Medical Institute. We thank B. Lassalle, J. Yano, and V. Yachandra for obtaining the x-ray absorption spectroscopy spectra; J. Breen for fabrication of electrochemical cells; Y. Hwang for assistance with gas chromatography; A. T. Iavarone for obtaining the mass spectra; and the University of California President's Postdoctoral Fellowship program for support of E.M. Structural parameters for **1** are available free of charge from the Cambridge Crystallographic Data Centre under identification number CCDC-798834. A patent has been filed by Lawrence Berkeley National Laboratory based on the results presented herein.

Supporting Online Material

www.sciencemag.org/cgi/content/full/335/6069/698/DC1
Materials and Methods
Figs. S1 to S14
Tables S1 and S2
References

27 October 2011; accepted 22 December 2011
10.1126/science.1215868

Near-Field Deformation from the El Mayor–Cucapah Earthquake Revealed by Differential LIDAR

Michael E. Oskin,[1]* J Ramon Arrowsmith,[2] Alejandro Hinojosa Corona,[3] Austin J. Elliott,[1] John M. Fletcher,[3] Eric J. Fielding,[4] Peter O. Gold,[1] J. Javier Gonzalez Garcia,[3] Ken W. Hudnut,[5] Jing Liu-Zeng,[6] Orlando J. Teran[3]

Large [moment magnitude (M_w) ≥ 7] continental earthquakes often generate complex, multifault ruptures linked by enigmatic zones of distributed deformation. Here, we report the collection and results of a high-resolution (≥nine returns per square meter) airborne light detection and ranging (LIDAR) topographic survey of the 2010 M_w 7.2 El Mayor–Cucapah earthquake that produced a 120-kilometer-long multifault rupture through northernmost Baja California, Mexico. This differential LIDAR survey completely captures an earthquake surface rupture in a sparsely vegetated region with pre-earthquake lower-resolution (5-meter–pixel) LIDAR data. The postevent survey reveals numerous surface ruptures, including previously undocumented blind faults within thick sediments of the Colorado River delta. Differential elevation changes show distributed, kilometer-scale bending strains as large as $\sim 10^3$ microstrains in response to slip along discontinuous faults cutting crystalline bedrock of the Sierra Cucapah.

Over the past century, most damaging continental earthquakes have arisen from multifault ruptures along incompletely mapped fault arrays (*1*). Quantifying this hazard is limited by inadequate understanding of the mechanisms by which faults link together to generate large earthquakes (*2*) and the difficulty of deducing large, multisegment events from paleoseismic records of ancient fault slip (*3*). Observations of fresh earthquake surface ruptures are critical to unraveling these problems because these most clearly illuminate relations between the paleoseismic record of faulting (at the surface) and seismic energy release that occurs predominantly at depth. In addition to the role of geometric fault segmentation in controlling the potential sizes of earthquakes (*3*), other important relations include the distribution of slip with depth (*4*, *5*) and the related problem of distributed deformation adjacent to faults (*5*–*8*). Well-studied earthquake surface ruptures in California (*9*–*11*) and elsewhere (*12*–*15*) have shown that earlier geologic observations may miss essential components of fault-zone deformation and underestimate the potential for ruptures to jump between faults.

The 4 April 2010 El Mayor–Cucapah sequence is a recent example of a large earthquake generated by a complex, multisegment fault rupture (*16*, *17*). Several faults—many but not all of which were mapped previously (*18*, *19*)—linked together to produce this moment magnitude (M_w) 7.2 earthquake. Because most evidence for ancient fault activity comes from the disruption of landforms by meter-scale fault slip, high-resolution light detection and ranging (LIDAR) topographic surveys (>1 sample/m^2) are valuable for delineating the extent of ancient ruptures, the detailed geometry and offsets in recent earthquakes (*20*), and, thus, the types of earthquakes that are likely to occur in the future. By immediately surveying the El Mayor–Cucapah surface rupture and comparing these measurements to pre-event LIDAR topography collected in 2006 by the Instituto Nacional de Estadística y Geografía (INEGI), we quantify both slip and spatially distributed warping associated with the faults that ruptured together in this earthquake.

To examine differential motion of the ground surface due to the earthquake, we removed the geoid correction from the pre-event LIDAR and subtracted the resulting ellipsoid heights from postevent LIDAR smoothed over a 2.5-m–radius window (*21*). The resulting elevation-difference map shows apparent vertical motion of the ground surface (Fig. 1 and fig. S1). In areas of steep slopes,

---

[1] Department of Geology, University of California, Davis, 1 Shields Avenue, Davis, CA 95618, USA. [2] School of Earth and Space Exploration, Arizona State University, Tempe, AZ 85287–1404, USA. [3] Centro de Investigación Científica y de Educación Superior de Ensenada, Carretera Ensenada-Tijuana no. 3918, Zona Playitas, C.P. 22860, Ensenada, Baja California, México. [4] Jet Propulsion Laboratory, California Institute of Technology, 4800 Oak Grove Drive, Pasadena, CA 91109, USA. [5] United States Geological Survey, 525 South Wilson Avenue, Pasadena, CA 91106, USA. [6] National Key Laboratory of Earthquake Dynamics, Institute of Geology, China Earthquake Administration, 1# Huayanli, Dewai Avenue, Beijing 100029.

*To whom correspondence should be addressed. E-mail: meoskin@ucdavis.edu